Hydration Process of Cement in the Presence of a Cellulosic Additive. A Calorimetric Investigation

Francesca Ridi, Emiliano Fratini, Francesca Mannelli, and Piero Baglioni*

Department of Chemistry and Consorzio Interuniversitario per lo Sviluppo dei Sistemi a Grande Interfase (CSGI), University of Florence, Via della Lastruccia 3-Sesto Fiorentino, I-50019 Florence, Italy

Received: January 13, 2005; In Final Form: May 18, 2005

In the cement industry, the extrusion technique is used to produce flat shapes with improved resistance to compression. Extrusion is a plastic-forming process that consists of forcing a highly viscous plastic mixture through a shaped die. The material should be fluid enough to be mixed and to pass through the die, and on the other hand, the extruded specimen should be stiff enough to be handled without changing in shape or cracking. These characteristics are industrially obtained by adding cellulosic polymers to the mixture. The aim of this work is to understand the action mechanism of these additives on the major pure phases constituting a typical Portland cement: tricalcium silicate (C_3S), dicalcium silicate (C_2S), tricalcium aluminate (C_3A), and tetracalcium iron-aluminate (C_4AF). In particular, a methylhydroxyethyl cellulose (MHEC) was selected from the best-performing polymers for further study. The effect of this additive on the hydration kinetics (rate constants, activation energies, and diffusional constants) was evaluated by means of differential scanning calorimetry (DSC) while the hydration products were studied by using thermogravimetry-differential thermal analysis (TG-DTA), X-ray diffraction (XRD), and scanning electron microscopy (SEM). MHEC addition in calcium silicate pastes produces an increase in the induction time without affecting the nucleation-and-growth period. A less dense CSH gel was deduced from the diffusional constants in the presence of MHEC. Moreover, CSH laminar features and poorly structured hydrates were noted during the first hours of hydration. In the case of the aluminous phases, the additive inhibits the growth of stable cubic hydrated phases (C_3AH_6), with the advantage of the metastable hexagonal phases being formed in the earliest minutes of hydration.

Introduction

Anhydrous Portland cement is a rather complex material mainly constituted by four phases: tricalcium silicate, Ca_3SiO_5, dicalcium silicate, Ca_2SiO_4, tricalcium aluminate, $Ca_3Al_2O_6$, and tetracalcium iron-aluminate, $Ca_4Al_2Fe_2O_{10}$. According to the widely accepted cement-chemical notation, CaO, SiO_2, and H_2O become C, S, and H, respectively, and the single phases can be represented shortly as C_3S, C_2S, C_3A, and C_4AF. Calcium silicates (C_3S and C_2S) react in water to give the calcium silicate hydrate, CSH, amorphous gel[1] and the crystalline calcium hydroxide, CH, referred to as portlandite, which has a well-known hexagonal structure. The hydration reaction of C_3S is completed after 1 month, while C_2S reacts more slowly and takes more than a year to be fully hydrated. Tricalcium aluminate and tetracalcium iron-aluminate react with water to give several metastable phases that successively convert into a cubic structure, represented by the general formula $C_3(AF)H_6$. This structural change is well noticeable below 30 °C, while at higher temperature the conversion is so fast that only the cubic phase is produced. As a simple approximation, the reaction of tricalcium aluminate with water may be represented by the equation $C_3A + 6H \rightarrow C_3AH_6$.[2] This product comes from the rearrangement of more complex hydrates (e.g. C_4AH_{13} and C_2AH_8), formed as platelets with hexagonal symmetry,[3] or from an initial amorphous gel,[4] depending on the external conditions. The hydration products formed by the ferrite solid solution, C_4AF, are usually described as being similar to those formed by C_3A, with Fe^{3+} partly exchanged with Al^{3+}.[3] The aluminates hydration reaction is faster than that of the silicates, and it is concluded in a few hours.

Recently, the application of quasi-elastic neutron scattering to the investigation of the cement setting process has been reported for the hydration of the four different phases.[5−7] The time evolution of the translation dynamics of the nonreacted water has been characterized in detail through the β exponent and the average relaxation time in the framework of the "relaxing cage model". In particular, both parameters confirm a rapid water confinement in the case of aluminate pastes (C_3A and C_4AF), while, in the silicates' case (C_3S and C_2S), the confinement process is slower, in agreement with the different kinetic rates and developing hydration products.

The use of natural polymers as proteins or polysaccharides to improve building material characteristics and performance can be dated back to ancient times. Currently, synthetic polymers are used in the cement industry to change the cement characteristics to some extent, in order, for example, to increase the workability and fluidity or to adjust the air entrainment and the water retention.

The continuous extrusion of cement-based mixtures is one of the actual methods to produce sheets, bricks, spacers, sewer pipes, and similar objects. It is considered one of the most promising applications to obtain new cementitious materials, as considerably less energy is used during continuous extrusion than during production of conventional ceramic materials.

Extrusion is a processing technique that has been shown to impart high performance characteristics to fiber-reinforced

* To whom all correspondence should be addressed. Phone: +39 055 457-3033. Fax: +39 055 457-3032. E-mail: piero.baglioni@unifi.it. Website: www.csgi.unifi.it.

10.1021/jp050237n CCC: $30.25
Published on Web 07/07/2005

cementitious materials.[8] Basically, a highly viscous, plasticlike mixture is forced through a die, a rigid opening of desired cross section.

To make the extrusion process possible on cement pastes, an additive must be added to confer fluidity and plasticity to the final paste and to enable it to be passed through the die, extruded, and handled without changing in shape or cracking.

One of the best-performing classes of polymers used in this process is that of methylhydroxyethyl cellulose (MHEC). In the case of C_3S, the effect of MHEC has already been investigated by us using NMR[9] and it has been shown that the cellulosic additive interacts with the water present inside the paste. Under these conditions, the hydration process becomes more efficient as the water is gradually released from the cellulose ether to the calcium silicate.

In previous studies,[10,11] we have also shown the possibility of investigating the hydration of C_3S as a function of temperature and in the presence of different superplasticizers (SPs) by determining the amount of unreacted water (free water index, FWI) vs time and using a novel differential scanning calorimetry (DSC) method. In fact, the fraction of reacted C_3S, α, can be calculated from the DSC curves of freezable water melting, with α being inversely proportional to the experimental enthalpy of fusion of freezable water present in the C_3S/water paste. From the FWI parameter, the kinetic mechanism of the cement hydration process can be obtained, allowing a complete characterization of the hydration process. The effect of added polymer is then correlated to the kinetic parameters obtained for the nucleation and diffusion periods of the hydration process.

In this paper, we used DSC at different temperatures (10, 20, 30, and 40 °C) to follow the hydration kinetics (rate constant, activation energy, and diffusional constant). Differential thermal analysis (DTA) and X-ray diffraction (XRD) were used to provide evidence of the hydration products, and scanning electron microscopy (SEM) allowed underlining the morphological changes on the main four phases constituting an ordinary Portland cement powder.

Experimental Section

Synthetic tricalcium silicate (C_3S), dicalcium silicate (C_2S), tricalcium aluminate (C_3A), and tetracalcium iron-aluminate (C_4AF) were supplied as a gift by CTG, Italcementi Group, with BET specific surface areas of 0.44 ± 0.05 m^2/g, 0.60 ± 0.05 m^2/g, 0.48 ± 0.05 m^2/g, and 0.54 ± 0.05 m^2/g and particles' median radii of 6.0 μm, 11.0 μm, 16.4 μm, and 12.4 μm, respectively.

MHEC was obtained from Bayer with the commercial name Walocel MKX 40 000 PP 0.1, a degree of substitution[12] (DS) of 1.75, and a molar degree of substitution (MS) of 2. A 2% aqueous solution of Walocel MKX 40 000 PP 0.1 at 20 °C had a viscosity of 40 000 mPa s.

Samples for calorimetric and diffraction measurements were prepared with a 0.4 water/solid ratio by mass. Before preparing the polymer-added samples, MHEC was prehydrated and a 3.6% w/w solution was obtained: the silicate or aluminate powder was mixed with this gel and with pure water in order to produce a paste with a 0.4 water/solid ratio and with 0.27% of MHEC on powder weight. Water was purified with a Millipore Organex system ($R \geq 18$ MΩ cm).

DSC measurements were performed using a Perkin-Elmer calorimeter DSC7, connected to a personal computer; data were elaborated with Pyris software for Windows, version 3.52. The paste (roughly 40 mg) was transferred in a steel pan (diameter 7.4 mm, capacity 60 μL, from Perkin-Elmer) that was sealed with the appropriate cover equipped with a neoprene O-ring to avoid water leaking. Each sample was maintained in a thermostatic bath at constant temperature (10, 20, 30, and 40 °C). Each measurement was carried out with the following temperature program: from room temperature down to −30 °C at 40 °C/min, isothermal regime at −30 °C for four minutes, from −30 °C to −12 °C at 20 °C/min, and from −12 °C to +14 °C at 4 °C/min. The isothermal step at −30 °C was performed to ensure that free water would freeze despite possible supercooling effects. Each DSC curve showed a peak relative to water freezing and a peak due to its melting. From the enthalpy variation of the water melting, we calculated the FWI according to the procedure reported in previous works.[10,11]

In the case of DTA and XRD, the hydration reaction was stopped in order to perform the investigation, since both techniques are affected by the presence of unreacted water. Several methods to stop the hydration reaction are reported in the literature[4,13−16] and are all based on the criterion that the unreacted water must be substituted by an organic solvent (easier to evaporate). According to a comprehensive review about the influence of the blocking protocol on the hydration mechanism of aluminates,[17] we applied the following procedure that we found to be the best: each sample was washed three times with ethanol and three times with a mixture of ethanol and ether (1:1 v/v), in order to remove the nonreacted water. At every washing step, the solvent was kept under stirring for 3 min and then the liquid part was discarded. The so-obtained wet solid was dried for 6 h at 40 °C in a nitrogen atmosphere.

DTA analysis was performed by using the SDT 2960, series Q600, TA instrument. The investigated temperature range was from 30 to 1000 °C with a rate increment of 15 °C/min.

XRD spectra were obtained using a D8 Advanced of Bruker AXS. Each spectrum was obtained by scanning from 10° to 90° with a step in 2θ equal to 0.02°, corresponding to an acquisition time of 1 h per spectrum. The spectra were elaborated using the EVA program, and the phase analysis was made using the ICDD Powder Diffraction File Database.

SEM observations were carried out by means of a JEOL-JSM 5600 working at 8−10 kV of acceleration potential. The preparation of the samples for SEM measurements was performed according to the procedure already described:[10] the samples were prepared with the same chemical compositions as those of the DSC experiments. Pastes were cured at 15 °C for the desired period and fractured and the inner part was chosen for SEM observation in order to have a sample representative of the bulk hydration and to avoid surface effects. The electron contrast was enhanced by coating the samples with a gold film with a JEOL Jee 4B apparatus.

Results and Discussion

Figures 1 and 2 report the time evolution of the FWI obtained for C_3S pastes cured at 10, 20, 30, and 40 °C in pure water and in the aqueous MHEC solution, respectively. The curves have the characteristic shape of those for cement hydration, being composed of three different periods. FWI slowly decreases until time t_i, then a sharp fall corresponding to the onset of the nucleation-and-growth process is observed. A further change of slope can be clearly seen, indicating the beginning of the diffusional regime, at time t_d. The influence of the storage temperature on the duration of the induction (or "dormant") period is evident from the t_i values reported in Table 1.

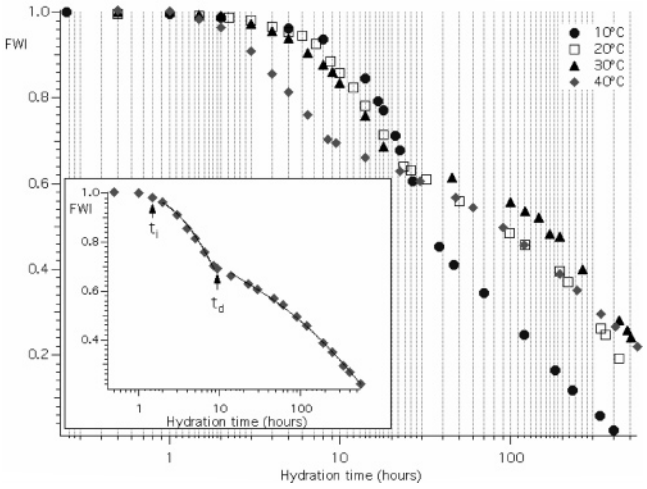

Figure 1. FWI vs time for a C_3S paste cured in pure water (w/c = 0.4) at 10, 20, 30, and 40 °C. As an example, in the inset, the fittings of the acceleration and diffusional periods are reported for the 40 °C curve.

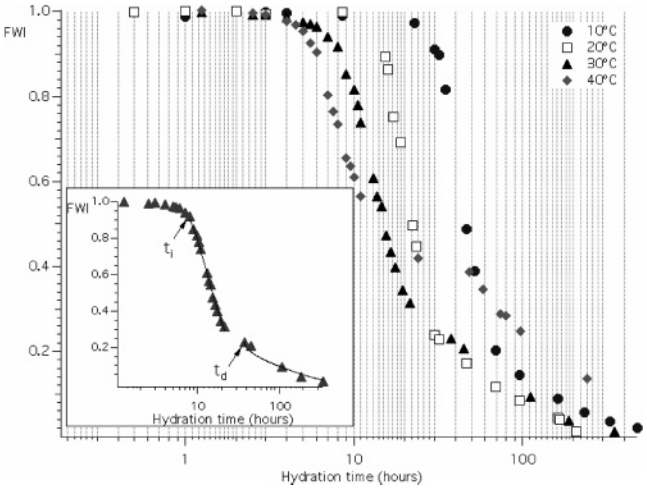

Figure 2. FWI vs time for a C_3S paste cured in water (w/c = 0.4) with MHEC at 10, 20, 30, and 40 °C. As an example, in the inset, the fittings of the acceleration and diffusional periods are reported for the 30 °C curve.

TABLE 1: Kinetic Parameters of the Nucleation-and-Growth Process and of the Diffusional Period for C_3S Hydration in Pure Water and with MHEC at the Four Investigated Temperatures

		nucleation-and-growth			diffusion-limited	
	T (°C)	t_i (h)	k (h^{-1})	M	t_d (h)	$K_d \times 10^{15}$ (m^2/h)
water	10	8	0.0113	1.3	38	13.7
water	20	6	0.0234	1.1	32	4.33
water	30	5	0.0271	1.0	18	3.72
water	40	1.5	0.0579	1.1	9.5	2.99
MHEC	10	32	0.0296	1.1	69.5	4.55
MHEC	20	15	0.0664	1.2	47	6.42
MHEC	30	8	0.0744	1.2	37.5	8.67
MHEC	40	6	0.1390	0.9	24	13.0

FWI was calculated from each measurement according to the following relationship:[10,11]

$$\mathrm{FWI} = \Delta H_{exp}/(\phi_{wt}\Delta H_{theor}) \quad (1)$$

where ΔH_{exp} corresponds to the area of the peak of water melting, ϕ_{wt} is the average weight fraction of water in the pastes, and ΔH_{theor} is the theoretical value of the fusion enthalpy of water in the C_3S/water paste. In the previous work, immediately after mixing, ΔH_{theor} was found to be approximately 85% of the value of pure water (333 J/g), in agreement with the influence of the sample's heterogeneity on the enthalpy changes as determined by DSC.[18] For this reason, extracted FWI values were corrected by this factor and, as a result, each curve starts from unity at the beginning of the hydration reaction.

As previously described,[10] the Avrami−Erofeev (A−E) model accounts for the nucleation process.[19−21] According to the A−E law, the variation of α (degree of reaction) in time is

$$\alpha = 1 + \alpha_i - e^{-k(t-t_i)^M} \quad (2)$$

where t_i is the initial time of the acceleration period, α_i is the degree of reaction at time t_i, k is the rate constant, and M is a parameter dependent on the dimensionality and the type of growth of the forming particles.

The previous equation can be linearized and written in the form

$$\ln\left[\ln\left(\frac{1}{1+\alpha_i-\alpha}\right)\right] = \ln k + M \ln(t - t_i) \quad (3)$$

In this way, given t_i, both k and M can be obtained from a linear least-squares fitting on the linear region of the plot.

The stoichiometric coefficients involved in the hydration reaction of C_3S are known to vary in time, and these variations should be taken into account to obtain a relation between FWI and the degree of reaction. However, according to Fuji and Kondo,[22] the hydration reaction can be simplified in the following form:

$$Ca_3SiO_5 + 3.9H_2O \rightarrow (CaO)_{1.68}\cdot(SiO_2)\cdot(H_2O)_{2.58} + 1.32Ca(OH)_2 \quad (4)$$

In this way, the relation between FWI and the degree of reaction, α, can be simply written as[22,23]

$$(1 - \mathrm{FWI}) = \frac{3.9\alpha}{12.7(w/c)} \quad (5)$$

where 12.7 is the ratio between the molecular weights of C_3S and H_2O and w/c is the water/cement ratio in weight. Since in our case w/c is kept constant and equal to 0.4, the relation can be further simplified as

$$\alpha = 1.3(1 - \mathrm{FWI}) \quad (6)$$

Each experimental curve has been fitted according to the A−E law, and the rate constants deduced from the fitting are listed in Table 1. The comparison of both the curves and the data obtained for the C_3S/water/MHEC paste with those of the C_3S/water paste shows that the presence of the cellulosic additive during the C_3S hydration produces two main effects. The first effect is a slight delay in the setting of C_3S paste: both the induction times, t_i, and the deceleration times, t_d, are increased when the cellulose ether is added to the paste, even if in a minor proportion to the superplasticizing additives.[11] The second effect is an improved hydration efficiency through an increased availability of the water in the hydration reaction, as already evidenced by NMR.[9] For example, in the case of the C_3S/water/MHEC paste cured at 20 °C, the acceleration period ends when only 20% of the water remains unreacted (FWI = 0.2), whereas, for the C_3S/water paste cured at the same temperature, the water remains nearly 60% unreacted, meaning that, in the presence of cellulose ether, the C_3S can react with most of the available water to complete the hydration reaction.

TABLE 2: Activation Energies for the Induction Period and for the Acceleratory Stage of the Hydration of C_3S in Pure Water and in the Presence of MHEC

	E_i (kJ/mol)	E_a (kJ/mol)
water	38	37
MHEC	42	35

As previously noted,[10,11,24] t_i values follow an Arrhenius-type behavior and the activation energies for the induction process have been calculated. The activation energy for the induction period of the paste containing MHEC is 42 kJ/mol. Since the corresponding value for the C_3S cured in pure water is 38 kJ/mol, we can assert that only a slight effect on the temperature dependence of the induction time at which the cement hydration reaction starts is produced when the cellulose ether is added to the system.

The analysis of Table 1 indicates that rate constants, k, are temperature-dependent and, in particular, increase with temperature. Activation energies can be easily obtained from the Arrhenius equation by plotting $\ln(k)$ vs $1/T$:

$$k(T) = A \exp(-E_a/RT) \tag{7}$$

In the presence of cellulosic polymer, the activation energy for the nucleation and growth process is essentially equal to that obtained with pure water. A value of 35 kJ/mol is estimated for the MHEC-added paste, not meaningfully different from the value of 37 kJ/mol for the C_3S/water system. This result indicates that cellulose ether, in contrast to superplasticizers (SPs),[11] does not affect the hydration thermodynamics; that is, the MHEC/C_3S interaction is negligible. However, the significant influence of this additive on the water availability suggests that, due to its highly hydrophilic chemical structure, it strongly interacts with the aqueous phase. Table 2 summarizes the activation energies for the induction and the acceleration periods of the two systems.

Furthermore, the analysis of the M value does not show any relevant change in comparison with the case of C_3S hydrated in pure water. According to the classical Avrami's nucleation-and-growth theory,[19−21] this parameter combines the time dependences of the nucleation-and-growth processes and is therefore related to the morphological characteristics of the growing crystals through the following relation:[23,25]

$$M = (P/S) + Q \tag{8}$$

where P is the dimensionality constant for the given kinetic process (it can be equal to 1, 2, or 3, corresponding to the growth of fibers, sheets, or polygonal forms, respectively); S is related to the rate-limiting growth mechanism (it is 1 for a phase boundary growth or 2 when the growth is controlled by diffusion through the liquid phase); and, finally, Q is a nucleation rate constant which in its limiting cases may be equal to 0 for no nucleation dependence (or nucleation sites saturation), whereas Q equal to 1 indicates a constant nucleation rate.

The M average value is around unity, both for C_3S/water and for C_3S/water/MHEC systems, and it is, therefore, consistent with two different morphological characteristics of the growing hydrates: (i) fibers−phase boundary−no nucleation, $P = 1$, $S = 1$, and $Q = 0$, also reported in the literature as (1,1,0); (ii) sheets−diffusion−no nucleation, $P = 2$, $S = 2$, and $Q = 0$, (2,2,0). It is worth remarking that the reported calorimetric approach does not assess any information in the nanoscale dimension and that P, S, and Q parameters only refer to the overall morphology of the growing nuclei. As atomic force microscopy (AFM) recent studies have plainly shown, the particles in the micrometer length scale are actually aggregates of much smaller platelike units. [26,27] The classical nucleation-and-growth theory applied on our DSC results does not contradict these recent AFM findings.

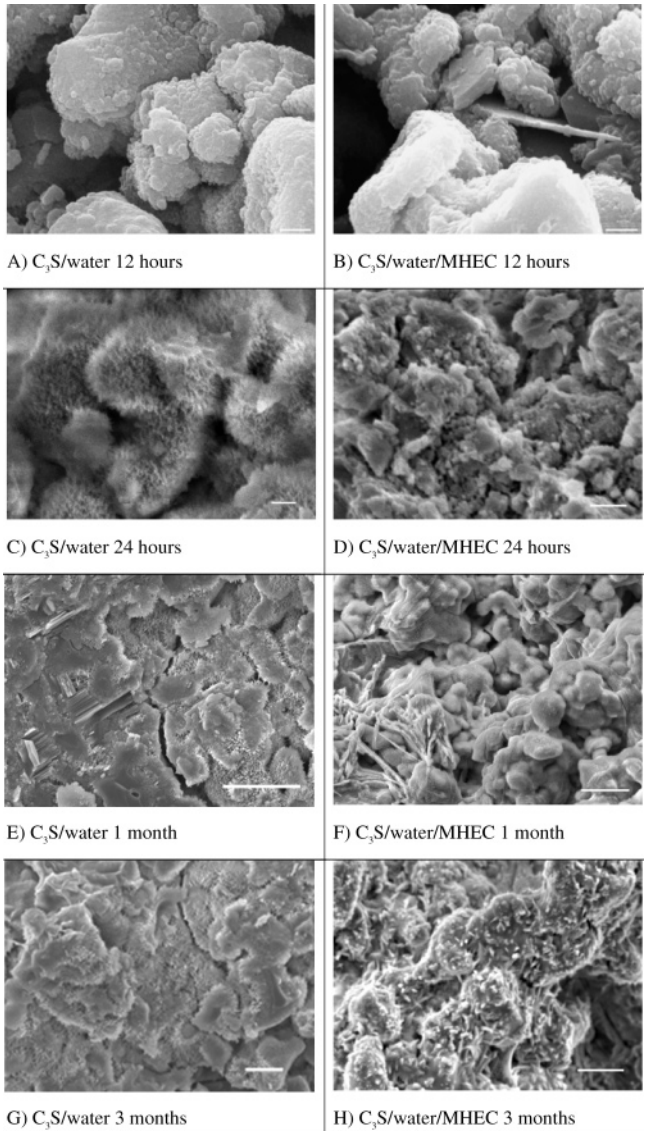

Figure 3. SEM micrographs of C_3S pastes (w/c = 0.4): (A) bar = 2 μm; (B) bar = 2 μm; (C) bar = 1 μm; (D) bar = 2 μm; (E) bar = 10 μm; (F) bar = 10 μm; (G) bar = 5 μm; (H) bar = 5 μm.

The SEM micrographs performed on pastes of C_3S cured in pure water reveal a one-dimensional microstructure of the CSH growing on the particle surfaces, in full accordance with the literature.[10,25,28,29] The presence of MHEC in the paste produces some significant modification in the appearance of the sample surfaces. The micrographs in Figure 3A and B show that no relevant difference between this system and the C_3S/water paste can be detected until 12 h; on the contrary, at higher hydration times (Figure 3C and D), the fibrils of the typical CSH growing phase are not present in the C_3S/water/MHEC pastes, suggesting that the presence of the additive affects the shape of the hydrated CSH. In the case of the SP compounds, this effect has been ascribed to the direct interaction of the additives with the C_3S surface.[11] In a recent article,[9] NMR relaxation times (longitudinal and transversal) for C_3S/water and C_3S/MHEC/water systems were discussed and compared with the relaxation times of the MHEC/water mixture. T_1 and T_2 trends provided evidence of the strong interaction between the water and the cellulosic

polymer. In particular, values of $T_1 = 950$ ms and $T_2 = 4$ ms have been found at the initial stage of the reaction in the C_3S/water paste and are reported in the literature as indicative of water constrained in capillary pores. The induction period of C_3S/water/MHEC is characterized by $T_1 = 1.18$ s and $T_2 = 6$ ms, essentially the same as those for water entrapped in MHEC alone ($T_1 = 1.23$ s and $T_2 = 5.75$ ms). This result supports the hypothesis of a strong interaction between the water and the cellulosic molecules inside cementitious pastes. It is also evident that this interaction significantly modifies the CSH morphology. The presence of the cellulosic polymer also changes the appearance of fully hydrated C_3S pastes, as evidenced by the micrographs obtained on samples cured for 1 month (Figure 3E and F) and 3 months (Figure 3G and H): the samples containing MHEC are much more compact with respect to standard pastes.

When all the external part of C_3S particles has reacted and CSH can no longer be formed on the surface, the hydration continues toward the interior of the grains. Under these conditions, the reaction rate is controlled by the diffusion of water across the CSH gel phase. The relation between the nonreacted water fraction (FWI) and time is the following:[22−24]

$$\mathrm{FWI}^{1/3} = -(2K_d)^{1/2}(t - t_d)^{1/2}/R + (\mathrm{FWI}_d)^{1/3} \qquad (9)$$

where K_d is the diffusional constant, t_d is the initial time of the diffusional period, FWI_d is the value of FWI relative to t_d, and R is the median radius of the particles.

For each curve, data with time greater than t_d (see Table 1) were considered to follow eq 9. It is evident that the diffusional constant K_d (listed in Table 1) can be calculated from the slope of the linear plot $\mathrm{FWI}^{1/3}$ vs $(t - t_d)^{1/2}$. The values obtained for pastes of C_3S in pure water are very similar to those reported in a previous work with neutron scattering, utilizing the same w/c ratio and similar surface area of the powder,[24] further confirming the validity of the method proposed here. Several studies showed K_d values to be independent of temperature.[10,24] This is attributed to the competition between two different contributions, the thermal activation of the diffusional process and the higher density of the gel phase at higher temperatures.[10,24,30,31] In fact, the diffusional constants would tend to increase with temperature because of the first contribution; however, the higher the temperature, the more impervious the "walk" of molecules across the medium, with a consequent decrease of diffusional constants.

As already noted,[11] the decreasing trend of the K_d observed for C_3S hydration in pure water, as the temperature increases, indicates that the structure of the hydrated phase becomes more impervious, hindering the water diffusion through it. When C_3S is hydrated in the presence of MHEC, the trend of the diffusional constants is exactly the opposite. K_d has been found to increase with the temperature, confirming the controlled release effect of MHEC on the hydration and indicating that the ordinary thermal activation is not affected by the disorder of the CSH matrix.

Dicalcium silicate, C_2S, is characterized by an extremely slow hydration process. It takes more than one year to complete the reaction. We acquired all of the kinetics for the hydration of this phase in pure water and in the presence of MHEC at 20 °C. The results are shown in Figure 4.

The shapes of the two curves (C_2S with and without additive) are similar, but MHEC is found to have a slightly retardant effect. Because of the slowness of the reaction, the C_2S system shows two different nucleation-and-growth periods, as it is evident from the two different slopes in the plot of the A−E law (Figure 5). For this reason, two different fittings have been applied to each curve. The end of the induction period occurs when 5% of the available water has reacted: this point marks, therefore, the t_i time relative to the first nucleation-and-growth period. The point where the slope changes indicates the initial time of the second nucleation-and-growth stage. The results of the fittings are summarized in Table 3.

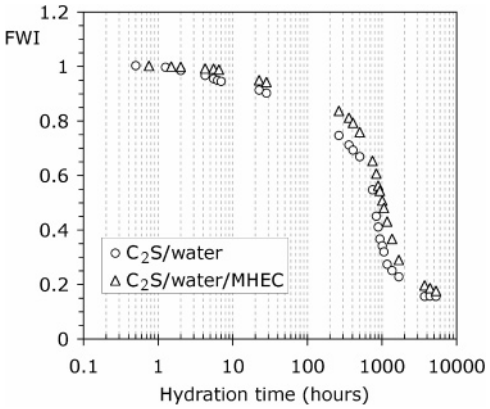

Figure 4. FWI vs time for a C_2S paste cured in water (w/c = 0.4) with (△) and without (○) MHEC at 20 °C.

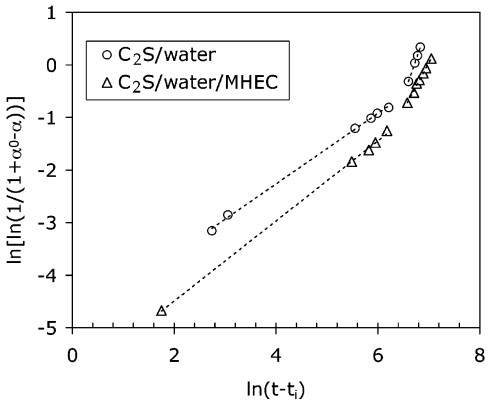

Figure 5. Avrami−Erofeev fittings for the nucleation-and-growth periods of C_2S pastes cured in water (w/c = 0.4) with (△) and without (○) MHEC at 20 °C.

TABLE 3: Parameters for the Nucleation-and-Growth Processes of C_2S Hydration in Pure Water and with MHEC at 20 °C

	t_i (h)	k (h^{-1})	M
water−1°	7	0.0071	0.7
water−2°	743	0.0036	0.8
MHEC−1°	22.5	0.0025	0.8
MHEC−2°	743	0.00063	1.0

Thermogravimetry−differential thermal analysis (TG-DTA) and XRD measurements (data not shown) performed on C_3S and C_2S powders in pure water and added with MHEC further confirm the previously described effect of the cellulose ether on the hydration kinetics. The formation of CSH and $Ca(OH)_2$ (whose decompositions occur at 120 °C and 450 °C, respectively) is detected in both the silicate pastes, and the presence of the additive does not change the chemical nature of the hydration products: nevertheless, a slight retardation is recorded when the MHEC is added to the mix.

The attempt to obtain reproducible curves by means of DSC for the C_3A hydration failed. This was expected considering the extremely high hydration heat developed upon the contact of this phase with water (850 J/g) that makes the control of the temperature during the sample preparation very hard. In contrast

to the C_3A case, the time evolution of FWI in the C_4AF/water and C_4AF/water/MHEC systems is reproducible, due to the lower hydration heat of C_4AF (420 J/g). However, as already specified, the nature of the hydrated phases for the aluminates is temperature-dependent, and the hydration behavior of these phases with the temperature is anomalous with respect to C_3S. In particular, the hydration rate increases as the temperature passes from 10 to 30 °C (data not shown); a further increment of the curing temperature up to 40 °C produces a decline in the hydration rate, in complete agreement with the literature.[32,33] Moreover, the FWI value obtained after the first minutes of hydration is extremely low. During the first 15 min, approximately 50% of the water reacts with the solid phase, becoming immediately undetectable with our method. Because of these reasons, it seems obvious that the DSC approach is partly appropriate to inspect the cellulose ether influence on C_3A and C_4AF hydration, since the earliest minutes of the reaction are decisive.

We utilized TG-DTA measurements to investigate the MHEC influence on the aluminate phases. We examined samples of C_3A and C_4AF powders mixed at 15 °C with water and with and without MHEC, and we observed the time evolution of the thermal effects produced from the decomposition of the hydrated phases. Particular attention was paid to the early stages of the process when most of the water is consumed in the heterogeneous reaction with the rapid formation of hydrated phases.

As an evidence of the extremely high reaction rate of the aluminate phases, it has to be noted that immediately after the mixing of both C_3A and C_4AF with water some reaction products are formed (Figures 6 and 7). Just after 5 min, the C_3A/water system presents two peaks at 128 °C and 280 °C (Figure 6A): with the progress of the hydration, the intensity of this latter peak increases, with a corresponding progressive shift toward higher temperature, up to 316 °C, after 4 days of curing. Previous studies performed on aluminoferrites[34] and on metakaolin[35] assign the decomposition occurring around 300 °C to stable cubic hydrogarnet phases. On the other hand, the XRD analysis performed on these samples effectively evidences the presence of C_3AH_6 (the cubic hydrogarnet product relative to the tricalcium aluminate hydration), together with some unreacted C_3A. No other XRD pattern is detectable, confirming the amorphous nature of the hydrated product responsible for the DTA peak at 128 °C.[4] The peak at 450 °C, registered on the sample cured for 4 days, is due to the loss of a remaining mole of crystal water from the hydrogarnet phase.[34]

When the MHEC is added to the paste (Figure 6B), a relevant inhibition in the formation of the cubic stable phase occurs in the first minutes of the reaction, as testified by the absence of the peak at 300 °C after 5 and 15 min from the mixing. These samples present endothermal features at 145, 230, and 260 °C. According to the XRD spectra, the hydrated products formed under these conditions are not crystalline, since no additional pattern is present apart from that of the anhydrous tricalcium aluminate. The presence of the cellulose ether during the early stages of C_3A hydration stabilizes the amorphous gel, precursor of the stable C_3AH_6. At hydration times over 30 min, the thermograms are identical to those obtained for the C_3A/water system.

The thermograms for the C_4AF/water and C_4AF/water/MHEC systems show decompositions approximately at the same temperatures previously reported for the C_3A hydration, indicating that the reaction mechanism of the two aluminate phases is the same. When C_4AF is incubated with pure water (Figure 7A), the formation of the cubic product ($C_3(AF)H_6$) is retarded with respect to the case of the tricalcium aluminate system. On the contrary, the phases whose water loss occurs at 150 and 230 °C are present in a higher amount than those in the C_3A/water paste. Again, the XRD confirms the presence of the cubic hydrogarnet product and of the amorphous gel.

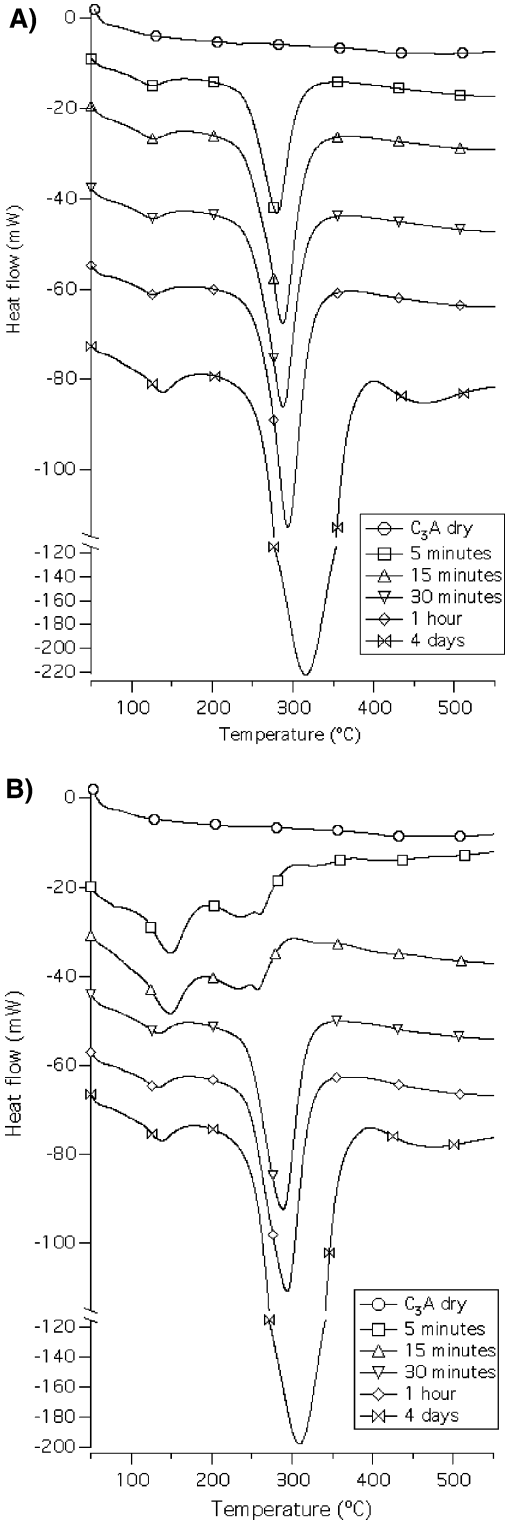

Figure 6. Temperature dependence of the heat flux for (A) C_3A/water and (B) C_3A/water/MHEC pastes after different times of hydration: 5 min (□), 15 min (△), 30 min (▽), 1 h (◇), and 4 days (⋈). The curve of dry C_3A has been reported as reference (○). An increasing negative offset has been added as a function of time for display purpose only.

MHEC influences the early stages of the C_4AF hydration in a striking way: it totally inhibits the growth of the stable C_3-

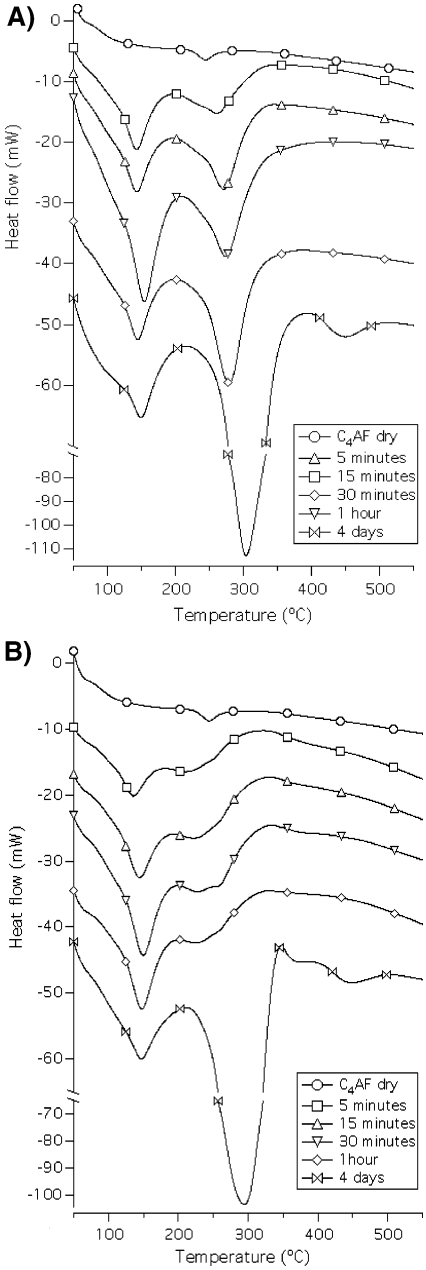

Figure 7. Temperature dependence of the heat flux for (A) C_4AF/water and (B) C_4AF/water/MHEC pastes after different times of hydration: 5 min (□), 15 min (△), 30 min (▽), 1 h (◇), and 4 days (⋈). The curve of dry C_4AF has been reported as reference (○). An increasing negative offset has been added as a function of time for display purpose only.

$(AF)H_6$ during the first hour after mixing. Only after 4 days of hydration are the decomposition peaks of the $C_3(AF)H_6$ (at 300 and 450 °C) recognizable (Figure 7B).

Figure 8 shows some micrographs obtained on the C_3A/water and C_3A/water/MHEC samples. C_3A cured in pure water for 5 min (Figure 8A) shows a compact and featureless structure. When the cellulose ether is added to the mix, the irregular foils, typical of the amorphous gel, appear. [4] When both the polymer-free and the polymer-added systems are cured for 1 h or more, their morphologies are dominated by the cubic phase, C_3AH_6. Figure 8C and D shows the structures after 4 days of hydration.

Similarly, the bulk of the C_4AF/water paste cured for 5 min appears as a featureless structure with some sporadic regions of irregular foils (Figure 9A). The cellulose ether produces a considerable stabilization of this acicular structure in the early

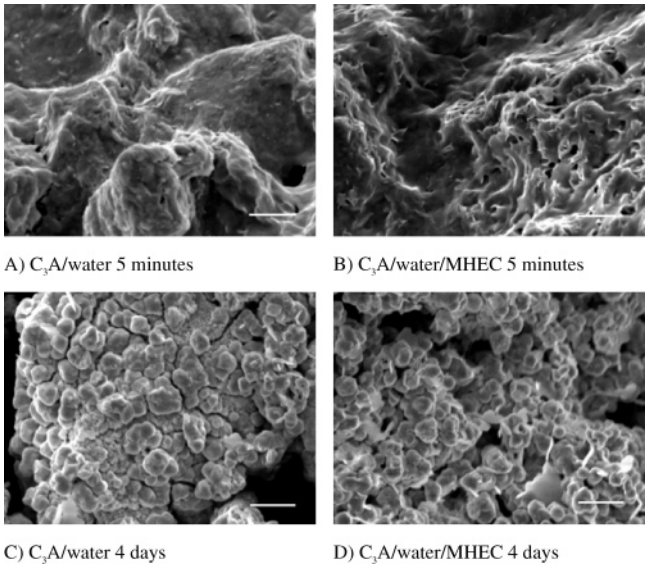

Figure 8. SEM micrographs of C_3A pastes (w/c = 0.4): bar = 5 μm.

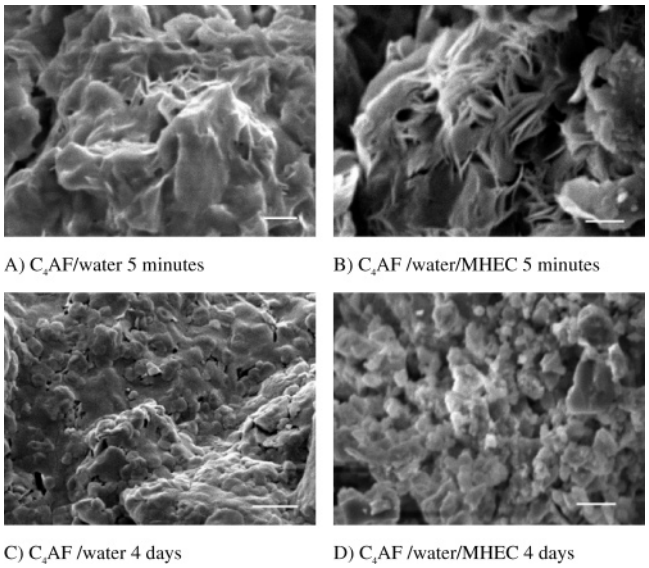

Figure 9. SEM micrographs of C_4AF pastes (w/c = 0.4): (A) bar = 2 μm; (B) bar = 2 μm; (C) bar = 5 μm; (D) bar = 2 μm.

stages of the C_4AF hydration: the samples cured both for 5 min (Figure 9B) and for 1 h (not shown) are characterized by these features. After 4 days, only the cubic phase is visible in both the systems (Figure 9C and D).

Conclusions

In the present work, the hydration of the main four phases constituting an ordinary Portland cement has been investigated. DSC allows us to perform an "in situ" analysis of the hydration kinetics of Ca_3SiO_5 (C_3S) and Ca_2SiO_4 (C_2S) phases in the presence of methylhydroxyethyl cellulose (MHEC). C_3S/water and C_3S/water/MHEC systems have been monitored at different temperatures (10, 20, 30, and 40 °C), in order to perform a complete kinetic analysis: the activation energies for the induction period and for the nucleation-and-growth process of the hydrated phase, the *M* parameter (related to the morphological characteristics of the growing crystals), and the diffusional constants have been obtained for these systems. The presence of cellulose ether does not significantly alter the activation energy for the acceleration period, and also, the *M* parameter remains roughly constant. These results indicate that no

modification in the C_3S hydration mechanism occurs in the presence of cellulose ether. However, FWI evolution highlights a strong increment of the water availability during the acceleration period, as a consequence of MHEC presence: the additive, due to its highly hydrophilic chemical structure, interacts with the aqueous phase, making it homogeneously distributed over the paste. As a consequence, the H_2O does not need to diffuse to reach the anhydrous C_3S and is available to the hydration in a shorter period of time. We also studied the hydration reaction at 20 °C of the C_2S phase with and without MHEC: in these systems, two steps in the formation of the hydrated phase can be identified. The rate constants of these two nucleation-and-growth periods have been calculated.

The evolution of the hydration reaction of $Ca_3Al_2O_6$ (C_3A) and $Ca_4Al_2Fe_2O_{10}$ (C_4AF) phases was monitored by differential thermal analysis (DTA): the MHEC was shown to stabilize the formation of the metastable amorphous aluminate hydrated gel in the early minutes of the reaction, with further inhibition of the formation of the stable phase, the cubic hydrogarnet $C_3(AF)H_6$. SEM was used to examine the morphological modifications occurring on the main four phases because of the presence of cellulose ether.

Acknowledgment. The authors thank Dr. L. Cassar, R. Alfani, G. Guerrini, M. Biagini (CTG-Italcementi Group), and L. Dei (CSGI) for their invaluable comments and discussions. Financial support from CTG-Italcementi Group, Ministero dell'Istruzione, Università e della Ricerca Scientifica (MIUR, Grant PRIN-2003), and Consorzio Interuniversitario per lo Sviluppo dei Sistemi a Grande Interfase, CSGI, is gratefully acknowledged.

References and Notes

(1) Xu, Z.; Viehland, D. *Phys. Rev. Lett.* **1996**, *77*, 952−955.
(2) Soroka, I. *Portland Cement Paste and Concrete*; The MacMillan Press LTD: 1979.
(3) Bye, G. C. *Portland cement. Composition, production and properties*, 2nd ed.; Thomas Telford: London, 1999.
(4) Breval, E. *Cem. Concr. Res.* **1976**, *6*, 129−138.
(5) Fratini, E.; Chen, S. H.; Baglioni, P.; Bellissent-Funel, M. C. *J. Phys. Chem. B* **2002**, *106*, 158−166.
(6) Fratini, E.; Chen, S. H.; Baglioni, P.; Cook, J. C.; Copley, J. R. D. *Phys. Rev. E* **2002**, *65*, 010201.
(7) Fratini, E.; Chen, S. H.; Baglioni, P. *J. Phys. Chem. B* **2003**, *107*, 10 057−10 062.
(8) Shao, Y.; Marikunte, S.; Shah, S. P. *Concr. Int.* **1995**, *17*, 48−52.
(9) Alesiani, M.; Capuani, S.; Giorgi, R.; Maraviglia, B.; Pirazzoli, I.; Ridi, F.; Baglioni, P. *J. Phys. Chem. B* **2004**, *108*, 4869−4874.
(10) Damasceni, A.; Dei, L.; Fratini, E.; Ridi, F.; Chen, S. H.; Baglioni, P. *J. Phys. Chem. B* **2002**, *106*, 11 572−11 578.
(11) Ridi, F.; Dei, L.; Fratini, E.; Chen, S. H.; Baglioni, P. *J. Phys. Chem. B* **2003**, *107*, 1056−1061.
(12) DS indicates the average number of etherified hydroxyl groups in a glucose unit, whereas MS indicates the average number of bonded hydroxyalkyl groups per monomer unit. While the maximum obtainable DS is 3 (number of hydroxyl groups in a glucose unit), MS has theoretically no limit, since ethylene oxide can form side chains during the reaction.
(13) Smith, A.; Chotard, T.; Gimet-Breart, N.; Fargeot, D. *J. Eur. Ceram. Soc.* **2002**, *22*, 2261−2268.
(14) Guirado, F.; Gali′, S.; Chincon, J. S. *Cem. Concr. Res.* **1998**, *28*, 381−390.
(15) Stoch, A.; Zdaniewicz, M.; Paluszkiewicz, C. *J. Mol. Struct.* **1999**, *511−512*, 319−325.
(16) Georgescu, M.; Puri, A.; Coarna, M.; Voicu, G.; Voinitchi, D. *Cem. Concr. Res.* **2002**, *32*, 1269−1275.
(17) Bachiorrini, A.; Guilhot, B. *Cem. Concr. Res.* **1982**, *12*, 559−567.
(18) Wendlandt, W. W. *Thermal analysis*, 3rd ed.; Wiley-Interscience: New York, 1986.
(19) Avrami, M. *J. Chem. Phys.* **1939**, *7*, 1103−1112.
(20) Avrami, M. *J. Chem. Phys.* **1940**, *8*, 212−224.
(21) Avrami, M. *J. Chem. Phys.* **1941**, *9*, 177−184.
(22) Fujii, K.; Kondo, W. *J. Am. Ceram. Soc.* **1974**, *57*, 492−497.
(23) Berliner, R.; Popovici, M.; Herwig, K. W.; Berliner, M.; Jennings, H. M.; Thomas, J. J. *Cem. Concr. Res.* **1998**, *28*, 231−243.
(24) FitzGerald, S. A.; Neumann, D. A.; Rush, J. J.; Bentz, D. P.; Livingston, R. A. *Chem. Mater.* **1998**, *10*, 397−402.
(25) Brown, P. W.; Pommersheim, J.; Frohnsdorff, G. *Cem. Concr. Res.* **1985**, *15*, 35−41.
(26) Garrault-Gauffinet, S.; Nonat, A. *J. Cryst. Growth* **1999**, *200*, 565−574.
(27) Nonat, A. *Cem. Concr. Res.* **2004**, *34*, 1521−1528.
(28) Double, D. D.; Hellawell, A. *Nature* **1976**, *261*, 486-488.
(29) Double, D. D.; Hellawell, A. *Nature* **1977**, *237*, 82−90.
(30) Escalante-Garcìa, J. I.; Sharp, J. H. *Cem. Concr. Res.* **1998**, *28*, 1245−1257.
(31) Massazza, F.; Daimon, M. Presented at 9th International Congress on the Chemistry of Cement, New Delhi, India, 1992.
(32) Capmas, A. In *Calcium Aluminate Cements*; Mangabhai, R. J., Ed.; E&FN Spon: London, 1990.
(33) Bushnell-Watson, S. M.; Sharp, J. H. *Cem. Concr. Res.* **1990**, *20*, 677−686.
(34) Csizmadia, J.; Balazs, G.; Tamas, F. D. *Cem. Concr. Res.* **2001**, *31*, 577−588.
(35) Rojas, M. F.; Sanchez de Rojas, M. I. *Cem. Concr. Res.* **2003**, *33*, 643−649.